IEEE Access
Multidisciplinary ⋮ Rapid Review ⋮ Open Access Journal

Received 13 September 2022, accepted 6 October 2022, date of publication 10 October 2022, date of current version 20 October 2022.

Digital Object Identifier 10.1109/ACCESS.2022.3213709

RESEARCH ARTICLE

Small-Signal Modeling and Interaction Analysis of LCC-HVDC Systems Based on Harmonic State Space Theory

KEZHENG JIANG, PAN HU, (Senior Member, IEEE), KAN CAO, DAN LIU, AND CHANG YE
State Grid Hubei Electric Power Research Institute, Wuhan, Hubei 430074, China

Corresponding author: Kezheng Jiang (jiangkz21@163.com)

This work was supported by the Science and Technology Project of State Grid Corporation of China under Project 5100-202199549A-0-5-ZN.

ABSTRACT High-voltage direct current (HVDC) technology based on Line Commutated Converter (LCC) is widely used in modern power systems due to its numerous benefits. However, as a typical power electronic device, LCC-HVDC has caused significant changes in the dynamic behavior of modern power systems due to largely replaced conventional power supplies in power systems. The interactions among sending-terminal and receiving-terminal system become stronger and have caused some stability issues, but the mechanism behind this has yet to be fully revealed. In order to analyze the interactions among sending-terminal and receiving-terminal system of LCC-HVDC, a small-signal model of modular HSS modeling is proposed based on Harmonic State Space (HSS) theory. Comparison of time-domain response with detailed switching model shows that the proposed can well reflect the dynamic behavior of the detailed switching model. Based on the model, the influence of controller's parameters on system stability is analyzed, as well as the dynamic interactions of LCC-HVDC among sending-terminal and receiving-terminal system are investigated. Analytical results demonstrate that there exists interactions among sending-terminal and receiving-terminal system which have an influence on the stability of the system.

INDEX TERMS Line commutated converter, sending-terminal and receiving-terminal system, interactions, harmonic state space, modular.

I. INTRODUCTION

In recent years, LCC-HVDC has been widely used in High-voltage direct current transmission project [1], [2], [3], due to its advantages of large capacity, long-distance transmission, lower line cost, etc. and plays an important role in power transmission [4]. With the widespread application of LCC-HVDC, the strength of AC system is relatively weakened and interactions between sending-terminal and receiving-terminal system get stronger [5], [6]. Under the weak networks, the problem of interactions among sending-terminal and receiving-terminal system which means the power devices interact with each other through sending-terminal and receiving-terminal system become prominent, and threaten the safety and stability of power system. Therefore, the accurate modeling and interactions analysis of the systems have become the focus of current research.

Some instability phenomena caused by interactions among sending-terminal and receiving-terminal system have been reported. On July 5th, 2013, a single-phase transient fault occurred in AC network of receiving-terminal system in shanghai of China. The disturbance was transferred to the sending-terminal system which led to the overvoltage and waveform distortions at the converter buses and low-voltage side of the station transformer [7]. The influence of commutation failure in receiving-terminal system on the system stability in sending-terminal system is analyzed in [8]. The modeling of LCC-HVDC and system stability of grid-connected system is studied in [9], [10], and [11]. In the analysis of system characteristics, the time-domain

The associate editor coordinating the review of this manuscript and approving it for publication was Inam Nutkani.

simulation method was applied earlier, but it has some disadvantages such as larger computation and difficult explanation of oscillation mechanism [12]. In order to reduce the computation of model of LCC-HVDC, the quasi-steady state model was established by simplifying the original relationship [13], although the simulation speed was improved, but the switching dynamics and DC current dynamics were ignored, so it was mainly used to analyze the influence of LCC-HVDC on low-frequency oscillation. In order to combine the requirements of simulation speed and dynamic analysis, the dynamic phasor model of LCC-HVDC was established based on Fourier series expansion and harmonic balance principle [14], [15], [16]. However, with the increase of the order considered, the complexity of the dynamic phasor model will increase sharply due to the nonlinearity of its controller and commutation process. Therefore, it is often used to analyze the stability of systems of lower order. In addition, in recent years, the impedance analysis has gradually become an effective method for small-signal modeling and stability analysis by its ''black box'' characteristics. The DC impedance model of LCC-HVDC is derived from the DC side of rectifier station and inverter station [17], and the harmonic stability characteristics of LCC-HVDC under the weak network are analyzed. However, the perspective of DC impedance model is only on the DC network, so it is difficult to analyze the interactions between converter station and AC network or other power electronic equipment. Recently, in order to solve the nonlinearity of controller and commutation process of LCC-HVDC, some scholars put forward a harmonic state space (HSS) model [18]. However, [18] doesn't analyze the factors that impacts the system's stability and the relationship between each link is not given.

The HSS theory was originally applied to single-phase two-level voltage source converter (VSC) system [19], [20], and then promoted to modular multilevel converter (MMC) system [21]. However, the HSS theory is rarely applied to LCC-HVDC. For the modeling of HSS, the most studies mainly deal with the state space equation of the system and realize it through programming [22]. As the system becomes more complex, the method is not conducive to the understanding and extension of the model. Therefore, this paper proposes the idea of modular HSS modeling, which is beneficial to understand the links that affect the stability of the system and the realization of visual analysis tools. Based on the above ideas, the linearization is applied to the nonlinear equations on the steady-state periodic trajectory of the LCC-HVDC, a small-signal model of modular HSS corresponding to each link of LCC-HVDC is established, and the influence of the controller's parameters on the system stability is investigated. By means of modal analysis, the dominant state variables causing the instability modes are studied, and analytical results demonstrate that there exists interactions among sending-terminal and receiving-terminal system which have an influence on the stability of the system.

The rest parts of this paper are organized as follows: The section II provides the physical topology and control of LCC-HVDC system. The section III provides a small-signal model of modular HSS of LCC-HVDC. Then, the influence of the controller's parameters and the interactions between the sending-terminal and receiving-terminal system on the system stability are analyzed in section IV. Section V draws the conclusions.

II. CONFIGURATION OF THE LCC-HVDC SYSTEM

This section mainly introduces the basic configuration of LCC-HVDC. Including physical topology and control scheme of LCC-HVDC.

A. PHYSICAL TOPOLOGY OF LCC-HVDC

FIGURE. 1 depicts the basic structure of two-terminal LCC-HVDC systems, which consists of five parts: the AC network of sending-terminal system, the rectifier station, the DC line, the inverter station and the AC network of receiving-terminal system. The rectifier/inverter station adopt a twelve-pulse converter, u_{sr} and u_{cr} represent the AC system voltage and AC bus voltage of sending-terminal system, respectively. L_{dcr} and L_{dci} represent the smoothing inductor, u_{si} and u_{ci} represent the AC system voltage and AC bus voltage of receiving-terminal system, respectively, k_{rT} represents the ratio of the rectifier station's transformer, k_{iT} represents the ratio of the inverter station's transformer.

B. CONTROL SCHEME OF LCC-HVDC

FIGURE. 2 is the control scheme of the sending-terminal system. The control scheme adopts the DC current control, and the PLL control provides the reference phase for the pulse generator, which produces pulse sequence together with the output of the DC current control. Typical proportional-integral (PI) regulators are applied in control loops of the sending-terminal system, β_r and α_{rord} represent the reference value of leading angle and firing angle of rectifier station, respectively, θ_{PLLr} is output phase of PLL of rectifier station.

FIGURE. 3 is the control scheme of the receiving-terminal system. The inverter station operates in DC voltage control whose output is the reference value of firing angle, and the PLL control provides the reference phase for the pulse generator, which produces pulse sequence together with the firing angle order, β_i and α_{iord} represent the reference value of leading angle and firing angle of inverter station, respectively, θ_{PLLi} is output phase of PLL of inverter station.

III. SMALL-SIGNAL MODELING OF THE LCC-HVDC SYSTEM

A. REVIEW OF LINEAR TIME PERIOD SYSTEMS THEORY AND HSS METHOD

The LCC-HVDC system is a nonlinear system due to the nonlinear characteristics of the switching circuit. Under steady-state operating conditions, the time-domain responses of both the AC system and the state variables of converter are characterized by time-periodic characteristics, In essence, the LCC-HVDC system is a nonlinear time-periodic system (NLTP). The idea of linear time-periodic (LTP) theory is

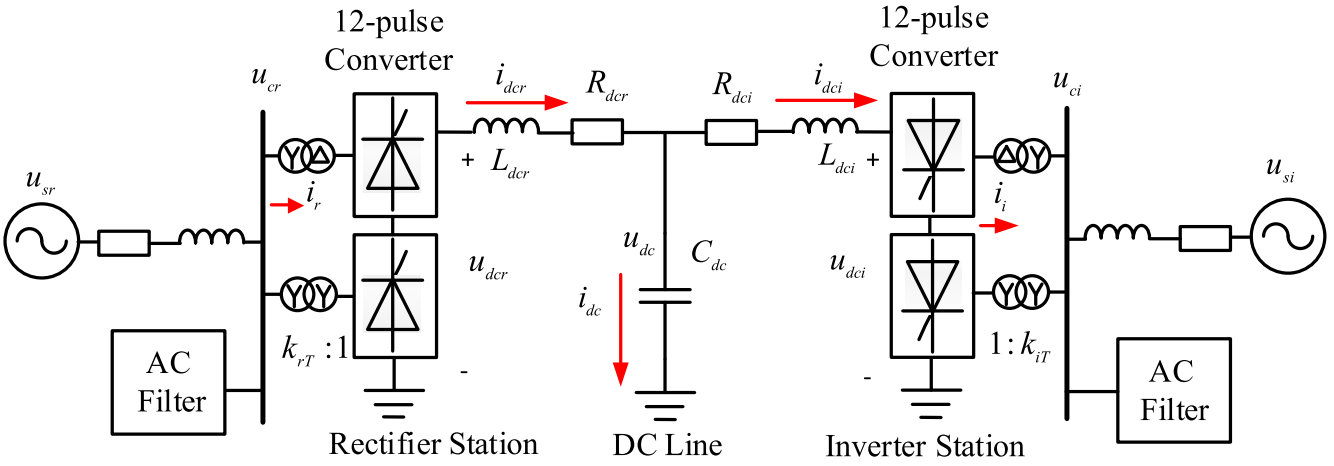

FIGURE 1. Main circuit of the two-terminal LCC-HVDC systems.

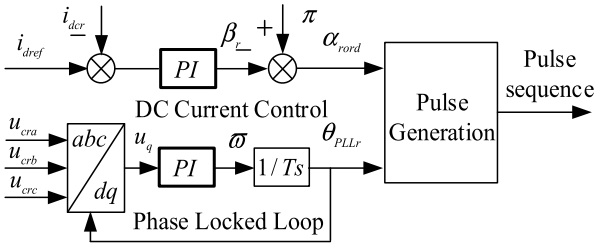

FIGURE 2. Control structure of rectifier.

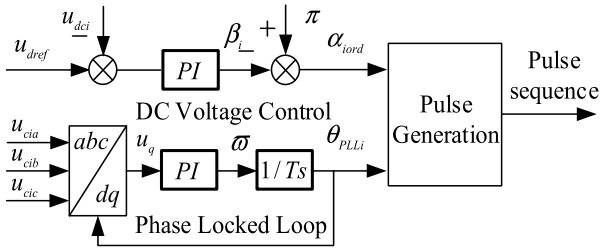

FIGURE 3. Control structure of inverter.

to linearize the nonlinear time periodic system at steady-state periodic trajectory rather than at an equilibrium point. The premise of system stability analysis is the modeling of LCC-HVDC system, some simplified models didn't consider the nonlinearity and periodic time-varying characteristics, which may lead to intrinsic errors in the analysis results. FIGURE 4 shows the idea for modeling nonlinear time-periodic system, the modular modeling proposed in this paper is to solve the nonlinearity and periodic time-varying challenge of controller and commutation process of LCC-HVDC, and to analyze dynamic interactions of LCC-HVDC among sending-terminal and receiving-terminal system on system stability.

For the linear time-periodic system, the equation of state can be expressed as:

$$\begin{cases} \dot{x}(t) = A(t)x(t) + B(t)u(t) \\ y(t) = C(t)x(t) + D(t)u(t) \end{cases} \tag{1}$$

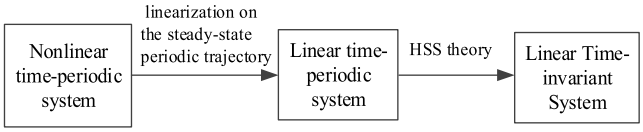

FIGURE 4. Idea for modeling nonlinear time-periodic system.

where $A(t)$, $B(t)$, $C(t)$ and $D(t)$ are time-periodic. For frequency analysis of LCC-HVDC system, both input variables and state variables are exponential modulating signals. Taking state variables as examples, they can be expressed as:

$$x(t) = e^{st}\sum_{-\infty}^{\infty} X_k e^{jk\varpi t} = \sum_{-\infty}^{\infty} X_k e^{(jk\varpi+s)t} \tag{2}$$

where X_k is the Fourier coefficient, k is the harmonics order, and ω is the fundamental angular frequency.

Similarly, the input signal can also be expressed in the form of complex exponential modulation

$$u(t) = e^{st}\sum_{-\infty}^{\infty} U_k e^{jk\varpi t} = \sum_{-\infty}^{\infty} U_k e^{(jk\varpi+s)t} \tag{3}$$

where U_k is the Fourier coefficient, k is the harmonics order.

Although $A(t)$, $B(t)$, $C(t)$ and $D(t)$ are functions of time t, there is no transient process. Taking matrix A as an example, it can be expressed as:

$$A(t) = \sum_{-\infty}^{\infty} A_k e^{jk\varpi t} \tag{4}$$

The state variables, input variables and matrix of the above formula expressed in the form of Fourier series are substituted into the equation of state of the system, which can be derived as

$$\sum_{k=-\infty}^{\infty} (jk\varpi + s)X_k e^{(jk\varpi+s)t}$$

$$= \sum_{k,m=-\infty}^{\infty} A_{k-m} X_m e^{(jk\varpi+s)t} + \sum_{k,m=-\infty}^{\infty} B_{k-m} U_m e^{(jk\varpi+s)t} \quad (5)$$

According to the harmonic balance principle, the components of the left and right sides of the above equation are taken at the same frequency, and the equation of state of the k harmonic can be obtained

$$(jk\varpi + s) X_k = \sum_{m=-\infty}^{\infty} A_{k-m} X_m + \sum_{m=-\infty}^{\infty} B_{k-m} U_m \quad (6)$$

k is used to represent the rows of the matrix, and m is used to represent the columns of the matrix. The harmonics of state variables and input variables are written into the matrix form according to the columns, and finally the harmonic state space (HSS) model can be obtained

$$sX = (\Gamma(A) - N) X + \Gamma(B) \boldsymbol{U} \quad (7)$$

where $X = [X_{-k}, \ldots, X_{-1}, X_0, X_1, \ldots, X_k]^T$, $U = [U_{-k}, \ldots U_{-1}, U_0, U_1, \ldots, U_{-k}]$, the elements in the column matrix are the Fourier coefficients of the variables, $N = diag[-jk\omega, \ldots -j\omega, 0, j\omega, \ldots jk\omega]$, $\Gamma(A)$ is the Toeplitz form of the $A(t)$ matrix, mapping the Fourier coefficient to an infinite matrix block, which can be expressed as

$$\Gamma(A) = \begin{bmatrix} \ddots & \vdots & \vdots & \vdots & \\ \ldots & A_0 & A_{-1} & A_{-2} & \ldots \\ \ldots & A_1 & A_0 & A_{-1} & \ldots \\ \ldots & A_2 & A_1 & A_0 & \ldots \\ & \vdots & \vdots & \vdots & \ddots \end{bmatrix} \quad (8)$$

The Toeplitz transform is introduced to simplify the algebraic operation of the sum and product of the Fourier series of functions and is also suitable for converting time-periodic ordinary differential equations or algebraic equations to invariant infinite-dimensional algebraic equations.

It is worth noting that the HSS model is in the frequency domain, and the conversion relationship with the time-domain can be expressed as:

$$x(t) = P(t)X \quad (9)$$

where $P(t) = [e^{-jk\omega}, \ldots e^{-j\omega}, 0, e^{j\omega}, \ldots e^{jk\omega}]$.

B. CONVERTER MODELING

The converter is an important component of LCC-HVDC. In this paper, taking the inverter station as an example, twelve-pulse converter is adopted considering the commutation process, the ratio of the transformer is considered of the model while the leakage inductance of transformer is ignored. The AC-DC relationship based on the switching function can be expressed as

$$\begin{cases} u_{dci} = (s_{iva} u_{cia} + s_{ivb} u_{cib} + s_{ivc} u_{cic})/k_{iT} \\ i_{ia} = s_{iia} i_{dci}/k_{iT} \\ i_{ib} = s_{iib} i_{dci}/k_{iT} \\ i_{ic} = s_{iic} i_{dci}/k_{iT} \end{cases} \quad (10)$$

s_{iva}, s_{ivb} and s_{ivc} are voltage switching functions of phase a, b and c of inverter station respectively, s_{iia}, s_{iib} and s_{iic} are current switching functions of phase a, b and c of rectifier station respectively, u_{dci} and i_{dci} represent the DC voltage and current of inverter station respectively, u_{cia}, u_{cib} and u_{cic} represent the AC bus voltage of phase a, b and c of inverter station respectively, i_{ia}, i_{ib} and i_{ic} represent the output AC current of phase a, b and c of inverter station respectively, the subscripts r and i represent the signals in rectifier side and inverter side, k_{iT} represents the ratio of the inverter station's transformer.

Taking the current switch function of valve 1 as an example:

$$s_{i1} = \begin{cases} (\theta - \alpha)/\mu \\ \theta \in [\alpha + 2k\pi, \alpha + \mu + 2k\pi] \\ 1 \\ \theta \in [\alpha + \mu + 2k\pi, \alpha + 2\pi/3 + 2k\pi] \\ 1 - (\theta - \alpha - n)/\mu \\ \theta \in [\alpha + 2\pi/3 + 2k\pi, \alpha + 2\pi/3 + 2k\pi + \mu] \\ 0 \\ \theta \in [\alpha + 2\pi/3 + 2k\pi + \mu, \alpha + 2(k+1)\pi] \end{cases} \quad (11)$$

where θ is the phase of voltage, α is the firing angle, μ is the commuting angle, n represents $2\pi/3$.

The AC-DC relationship is linearized on steady-state periodic trajectory of the original nonlinear time-periodic differential-algebraic equation:

$$\begin{cases} \Delta u_{dci} = (u_{cia0} \Delta s_{iva} + s_{iva0} \Delta u_{cia} + u_{cib0} \Delta s_{ivb} \\ \quad + s_{ivb0} \Delta u_{cib} + u_{cic0} \Delta s_{ivc} + s_{ivc0} \Delta u_{cic})/k_{iT} \\ \Delta i_{ia} = (i_{dci0} \Delta s_{ria} + s_{ria0} \Delta i_{dci}) \\ \Delta i_{ib} = (i_{dci0} \Delta s_{rib} + s_{rib0} \Delta i_{dci})/k_{iT} \\ \Delta i_{ic} = (i_{dci0} \Delta s_{ric} + s_{ric0} \Delta i_{dci})/k_{iT} \end{cases} \quad (12)$$

where Δ stands the disturbance around the steady-state periodic trajectory, and the subscript "0" means the steady-state periodic trajectory of the signal.

Using the HSS method described in the previous section, the small signal model of HSS can be obtained:

$$\begin{cases} \Delta \boldsymbol{u}_{dci} = (\Gamma(u_{cia0}) \Delta \boldsymbol{s}_{iva} + \Gamma(s_{iva0}) \Delta \boldsymbol{u}_{cia} + \Gamma(u_{cib0}) \Delta \boldsymbol{s}_{ivb} \\ \quad + \Gamma(s_{ivb0}) \Delta \boldsymbol{u}_{cib} + \Gamma(u_{cic0}) \Delta \boldsymbol{s}_{ivc} + \Gamma(s_{ivc0}) \Delta \boldsymbol{u}_{cic})/k_{iT} \\ \Delta \boldsymbol{i}_{ia} = (\Gamma(i_{dci0}) \Delta \boldsymbol{s}_{iia} + \Gamma(s_{iia0}) \Delta \boldsymbol{i}_{dci})/k_{iT} \\ \Delta \boldsymbol{i}_{ib} = (\Gamma(i_{dci0}) \Delta \boldsymbol{s}_{iib} + \Gamma(s_{iib0}) \Delta \boldsymbol{i}_{dci})/k_{iT} \\ \Delta \boldsymbol{i}_{ic} = (\Gamma(i_{dci0}) \Delta \boldsymbol{s}_{iic} + \Gamma(s_{iic0}) \Delta \boldsymbol{i}_{dci})/k_{iT} \end{cases} \quad (13)$$

C. PHASE-LOCKED LOOP MODELING

The goal of phase-locked loop synchronization technology is to make its output track the phase of the three-phase AC voltage on the grid side, and provide the phase for park transformation and pulse generator. When the system is disturbed, the phase of the power grid will have a certain dynamic, and the output phase of the phase-locked loop will also have a certain dynamic, which will affect the actual firing angle. Therefore, the output dynamics of the phase-locked loop must be considered in the HSS model of LCC HVDC, the basic structure of the phase-locked loop is given in FIGURE 3.

The original relationship can be expressed as:

$$\begin{cases} \begin{bmatrix} u_{i\alpha} \\ u_{i\beta} \end{bmatrix} = \boldsymbol{T} \begin{bmatrix} u_{cia} & u_{cib} & u_{cic} \end{bmatrix}^T, \\ \begin{bmatrix} u_{id} \\ u_{iq} \end{bmatrix} = \boldsymbol{P}_\theta \begin{bmatrix} u_{i\alpha} \\ u_{i\beta} \end{bmatrix} \\ \dfrac{d\theta_{plli}}{dt} = \omega_i \\ \dfrac{dx_{ipll}}{dt} = k_{iipll} u_{iq}, \quad \omega_i = x_{ipll} + k_{ippll} u_{iq} \end{cases} \tag{14}$$

where $\boldsymbol{T}$ is the Clark transformation, $\boldsymbol{P}_\theta$ stands the Park transformation.

Applying linearization on the steady-state periodic trajectory of phase-locked loop:

$$\begin{cases} \begin{bmatrix} \Delta u_{i\alpha} \\ \Delta u_{i\beta} \end{bmatrix} = \dfrac{2}{3} \begin{bmatrix} 1 & -1/2 & -1/2 \\ 0 & \sqrt{3}/2 & -\sqrt{3}/2 \end{bmatrix} \begin{bmatrix} \Delta u_{cia} \\ \Delta u_{cib} \\ \Delta u_{cic} \end{bmatrix} \\ \begin{bmatrix} \Delta u_{id} \\ \Delta u_{iq} \end{bmatrix} = \begin{bmatrix} u_{iq0} & \cos\theta_{ipll0} & \sin\theta_{ipll0} \\ -u_{id0} & -\sin\theta_{ipll0} & \cos\theta_{ipll0} \end{bmatrix} \\ \times \begin{bmatrix} \Delta\theta_{ipll} \\ \Delta u_{i\alpha} \\ \Delta u_{i\beta} \end{bmatrix} \\ \dfrac{d\Delta\theta_{ipll}}{dt} = \Delta\omega_i \\ \dfrac{d\Delta x_{ipll}}{dt} = k_{iipll}\Delta u_{iq}, \quad \Delta\omega_i = \Delta x_{ipll} + k_{ippll}\Delta u_{iq} \end{cases} \tag{15}$$

Using the HSS method described in the previous section, the small signal model of HSS can be obtained:

$$\begin{aligned} &\begin{bmatrix} \Delta \boldsymbol{u}_{i\alpha} \\ \Delta \boldsymbol{u}_{i\beta} \end{bmatrix} \\ &\quad = \frac{2}{3} \begin{bmatrix} \boldsymbol{I} & -\boldsymbol{I}/2 & -\boldsymbol{I}/2 \\ \boldsymbol{Z} & \frac{\sqrt{3}}{2}\boldsymbol{I} & -\frac{\sqrt{3}}{2}\boldsymbol{I} \end{bmatrix} \begin{bmatrix} \Delta \boldsymbol{u}_{cia} \\ \Delta \boldsymbol{u}_{cib} \\ \Delta \boldsymbol{u}_{cic} \end{bmatrix} \\ &\begin{bmatrix} \Delta \boldsymbol{u}_{id} \\ \Delta \boldsymbol{u}_{iq} \end{bmatrix} \\ &\quad = \begin{bmatrix} \Gamma(u_{iq0}) & \Gamma(\cos\theta_{ipll0}) & \Gamma(\sin\theta_{ipll0}) \\ \Gamma(-u_{id0}) & \Gamma(-\sin\theta_{ipll0}) & \Gamma(\cos\theta_{ipll0}) \end{bmatrix} \end{aligned} \tag{16}$$

$$\begin{aligned} &\times \begin{bmatrix} \Delta \boldsymbol{\theta}_{ipll} \\ \Delta \boldsymbol{u}_{i\alpha} \\ \Delta \boldsymbol{u}_{i\beta} \end{bmatrix} \\ &(s+\boldsymbol{N})\,\Delta \boldsymbol{\theta}_{ipll} \\ &\quad = \Delta \boldsymbol{\omega}_i \\ &(s+\boldsymbol{N})\,\Delta \boldsymbol{x}_{ipll} \\ &\quad = k_{iipll}\Delta \boldsymbol{u}_{iq} \\ &\Delta \boldsymbol{\omega} = \Delta \boldsymbol{x}_{ipll} + k_{ippll}\Delta \boldsymbol{u}_{iq} \end{aligned} \tag{17, 18}$$

where $\boldsymbol{I}$ represents the identity matrix with order 2k+1, and $\boldsymbol{Z}$ represents the zero matrix with order 2k+1.

D. DC VOLTAGE CONTROL MODELING

DC voltage control is applied to the inverter station controller, including sampling link and DC voltage PI link. The original relationship can be expressed as:

$$\begin{cases} u_{idif} = \dfrac{1}{1+T_i s} u_{dci} \\ \beta_{iord} = \left(k_{ip} + \dfrac{k_{ii}}{s}\right)\left(u_{idif} - u_{idref}\right) \end{cases} \tag{19}$$

where T_i represents the time constant, and u_{idref} represents the reference value of DC voltage.

Linearizing the above formula on the steady-state periodic trajectory

$$\begin{cases} \dfrac{d\Delta u_{idrf}}{dt} = \dfrac{1}{T_i}\left(\Delta u_{dci} - \Delta u_{idrf}\right) \\ \dfrac{d\Delta x_{dc}}{dt} = k_{ii}\left(\Delta u_{idref} - \Delta u_{idrf}\right) \\ \Delta\beta_{iord} = \Delta x_{dc} + k_{ip}\left(\Delta u_{idref} - \Delta u_{idrf}\right) \end{cases} \tag{20}$$

Appling the HSS method described in the previous section, the small signal model of HSS can be obtained:

$$\begin{cases} (s+\boldsymbol{N})\,\Delta \boldsymbol{u}_{idrf} = \dfrac{1}{T_i}\left(\Delta \boldsymbol{u}_{dci} - \Delta \boldsymbol{u}_{idrf}\right) \\ (s+\boldsymbol{N})\,\Delta \boldsymbol{x}_{dc} = k_{ii}\left(\Delta \boldsymbol{u}_{idref} - \Delta \boldsymbol{u}_{idrf}\right) \\ \Delta \boldsymbol{\beta}_{iord} = \Delta \boldsymbol{x}_{dc} + k_{ip}\left(\Delta \boldsymbol{u}_{idref} - \Delta \boldsymbol{u}_{idrf}\right) \end{cases} \tag{21}$$

E. DC LINE MODELING

The structure diagram of DC line is shown in FIGURE 1, and the relationship between DC voltage and DC current can be obtained:

$$\begin{cases} u_{dcr} = R_{dcr} i_{dcr} + L_{dcr}\dfrac{di_{dcr}}{dt} + u_{dc} \\ C_{dc}\dfrac{du_{dc}}{dt} = i_{dcr} - i_{dci} \\ u_{dc} = R_{dci} i_{dci} + L_{dci}\dfrac{di_{dci}}{dt} + u_{dci} \end{cases} \tag{22}$$

where u_{dcr} and i_{dcr} represent the DC voltage and current of rectifier station respectively, u_{dc} and i_{dc} represent the DC voltage and current of DC capacitor respectively.

By linearizing the above formula, a linearized model of DC line can be obtained:

$$\begin{cases} L_{dcr}\dfrac{d\Delta i_{dcr}}{dt} = \Delta u_{dcr} - R_{dcr}\Delta i_{dcr} - \Delta u_{dc} \\ C_{dc}\dfrac{d\Delta u_{dc}}{dt} = \Delta i_{dcr} - \Delta i_{dci} \\ L_{dci}\dfrac{d\Delta i_{dci}}{dt} = \Delta u_{dc} - R_{dci}\Delta i_{dci} - \Delta u_{dci} \end{cases} \tag{23}$$

The HSS small signal model of DC line can be obtained:

$$\begin{cases} (s+\boldsymbol{N})\,\Delta \boldsymbol{i}_{dcr} = \dfrac{1}{L_{dcr}}\left(\Delta \boldsymbol{u}_{dcr} - R_{dcr}\Delta \boldsymbol{i}_{dcr} - \Delta \boldsymbol{u}_{dc}\right) \\ (s+\boldsymbol{N})\,\Delta \boldsymbol{u}_{dc} = \dfrac{1}{C_{dc}}\left(\Delta \boldsymbol{i}_{dcr} - \Delta \boldsymbol{i}_{dci}\right) \\ (s+\boldsymbol{N})\,\Delta \boldsymbol{i}_{dcr} = \dfrac{1}{L_{dci}}\left(\Delta \boldsymbol{u}_{dc} - R_{dci}\Delta \boldsymbol{i}_{dci} - \Delta \boldsymbol{u}_{dci}\right) \end{cases} \tag{24}$$

F. AC NETWORK MODELING

The AC network of LCC-HVDC uses the CIGRE HVDC Benchmark[23].

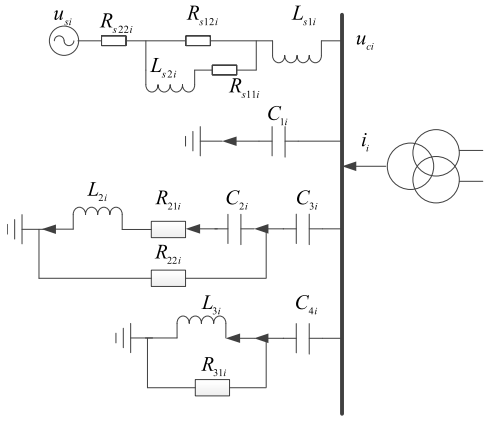

FIGURE 5. The structure of AC network.

The original relationship of ac network can be expressed as:

$$\frac{d}{dt}u_{cix} = K_{i11}u_{cix} + K_{i13}u_{c3ix} + K_{i14}u_{c4ix} + K_{i15}i_{2ix} + K_{i16}i_{3ix} + K_{i17}i_{1ix} + K_{i18}s_{iix}i_{dci}/k_{iT} \tag{25}$$

$$\frac{d}{dt}u_{c2ix} = K_{i25}i_{2ix} \tag{26}$$

$$\frac{d}{dt}u_{c3ix} = K_{i31}u_{cix} + K_{i33}u_{c3ix} + K_{i35}i_{2ix} \tag{27}$$

$$\frac{d}{dt}u_{c4ix} = K_{i41}u_{cix} + K_{i44}u_{c4ix} + K_{i46}i_{3ix} \tag{28}$$

$$\frac{d}{dt}i_{2ix} = K_{i51}u_{cix} + K_{i52}u_{c2ix} + K_{i53}u_{c3ix} + K_{i55}i_{2ix} \tag{29}$$

$$\frac{d}{dt}i_{3ix} = K_{i61}u_{cix} + K_{i64}u_{c4ix} \tag{30}$$

$$\frac{d}{dt}i_{s1ix} = K_{i71}u_{cix} + K_{i77}i_{s1ix} + K_{i78}u_{six} + K_{i79}i_{s2ix} \tag{31}$$

$$\frac{d}{dt}i_{s2ix} = K_{i87}i_{s1ix} + K_{i89}i_{s2ix} \tag{32}$$

where $K_{i11} \sim K_{i89}$ are invariants and will be given in TABLE 1. Linearizing the above formula on the steady-state periodic trajectory and using the HSS method described in the previous section, the HSS model of the AC network can be obtained:

$$\begin{aligned}(s+\boldsymbol{N})\,\Delta \boldsymbol{u_{cix}} = {} & \boldsymbol{K}_{i11}\Delta \boldsymbol{u_{cix}} + \boldsymbol{K}_{i13}\Delta \boldsymbol{u}_{c3ix} + \boldsymbol{K}_{i14}\Delta \boldsymbol{u}_{c4ix} \\ & + \boldsymbol{K}_{i15}\Delta \boldsymbol{i}_{2ix} + \boldsymbol{K}_{i16}\Delta \boldsymbol{i}_{3ix} + \boldsymbol{K}_{i17}\Delta \boldsymbol{i}_{1ix} \\ & + \boldsymbol{K}_{i18}\left(\boldsymbol{i}_{dci0}\Delta \boldsymbol{s_{iix}} + \boldsymbol{s}_{iix0}\Delta \boldsymbol{i_{dci}}\right)/k_{iT}\end{aligned} \tag{33}$$

$$(s+\boldsymbol{N})\,\Delta \boldsymbol{u}_{c2ix} = \boldsymbol{K}_{i25}\Delta \boldsymbol{i}_{2ix} \tag{34}$$

$$(s+\boldsymbol{N})\,\Delta \boldsymbol{u}_{c3ix} = \boldsymbol{K}_{i31}\Delta \boldsymbol{u_{cix}} + \boldsymbol{K}_{i33}\Delta \boldsymbol{u}_{c3ix} + \boldsymbol{K}_{i35}\Delta \boldsymbol{i}_{2ix} \tag{35}$$

$$(s+\boldsymbol{N})\,\Delta \boldsymbol{u}_{c4ix} = \boldsymbol{K}_{i41}\Delta \boldsymbol{u_{cix}} + \boldsymbol{K}_{i44}\Delta \boldsymbol{u}_{c4ix} + \boldsymbol{K}_{i46}\Delta \boldsymbol{i}_{3ix} \tag{36}$$

$$\begin{aligned}(s+\boldsymbol{N})\,\Delta \boldsymbol{i}_{2ix} = {} & \boldsymbol{K}_{i51}\Delta \boldsymbol{u_{cix}} + \boldsymbol{K}_{i52}\Delta \boldsymbol{u}_{c2ix} + \boldsymbol{K}_{i53}\Delta \boldsymbol{u}_{c3ix} \\ & + \boldsymbol{K}_{i55}\Delta \boldsymbol{i}_{2ix}\end{aligned} \tag{37}$$

$$(s+\boldsymbol{N})\,\Delta \boldsymbol{i}_{3ix} = \boldsymbol{K}_{i61}\Delta \boldsymbol{u_{cix}} + \boldsymbol{K}_{i64}\Delta \boldsymbol{u}_{c4ix} \tag{38}$$

$$\begin{aligned}(s+\boldsymbol{N})\,\Delta \boldsymbol{i}_{s1ix} = {} & \boldsymbol{K}_{i71}\Delta \boldsymbol{u_{cix}} + \boldsymbol{K}_{i77}\Delta \boldsymbol{i}_{s1ix} + \boldsymbol{K}_{i78}\Delta \boldsymbol{u_{six}} \\ & + \boldsymbol{K}_{i79}\Delta \boldsymbol{i}_{s2ix}\end{aligned} \tag{39}$$

$$(s+\boldsymbol{N})\,\Delta \boldsymbol{i}_{s2ix} = \boldsymbol{K}_{i87}\Delta \boldsymbol{i}_{s1ix} + \boldsymbol{K}_{i89}\Delta \boldsymbol{i}_{s2ix} \tag{40}$$

The HSS model of rectifier station can be also be obtained, which is similar to inverter station, it will not be expanded in detail.

G. TIME DOMAIN VALIDATION

This part verifies the accuracy of the modular HSS model of LCC-HVDC. According to the input-output relationship, the small-signal model of modular HSS of LCC-HVDC be obtained, and its structure is shown in FIGURE 6. In MATLAB/Simulink, the modular HSS model of LCC-HVDC was built, and the detailed switching model was built in PSCAD/EMTDC, the main parameters of LCC-HVDC are based on the CIGRE HVDC Benchmark. The simulation results of the modular HSS model are compared with the time-domain results of the detailed switching model to verify the accuracy. According to the harmonic state space theory, the HSS model has the characteristics of infinite order, in order to guarantee a good accuracy of the results, and at the same time, to keep low the computational complexity, we introduce a truncation order M which refers to the number of harmonics taken into account, a truncation order M=13 has been chosen because of the characteristics of the LCC-HVDC.

Initially, the system of rectifier station operates at $i_{dref} = 1.0$ pu, a small disturbance is applied to i_{dref} of -0.03 pu at 0.02s, the comparison of dynamic responses between detailed switching model and modular HSS model

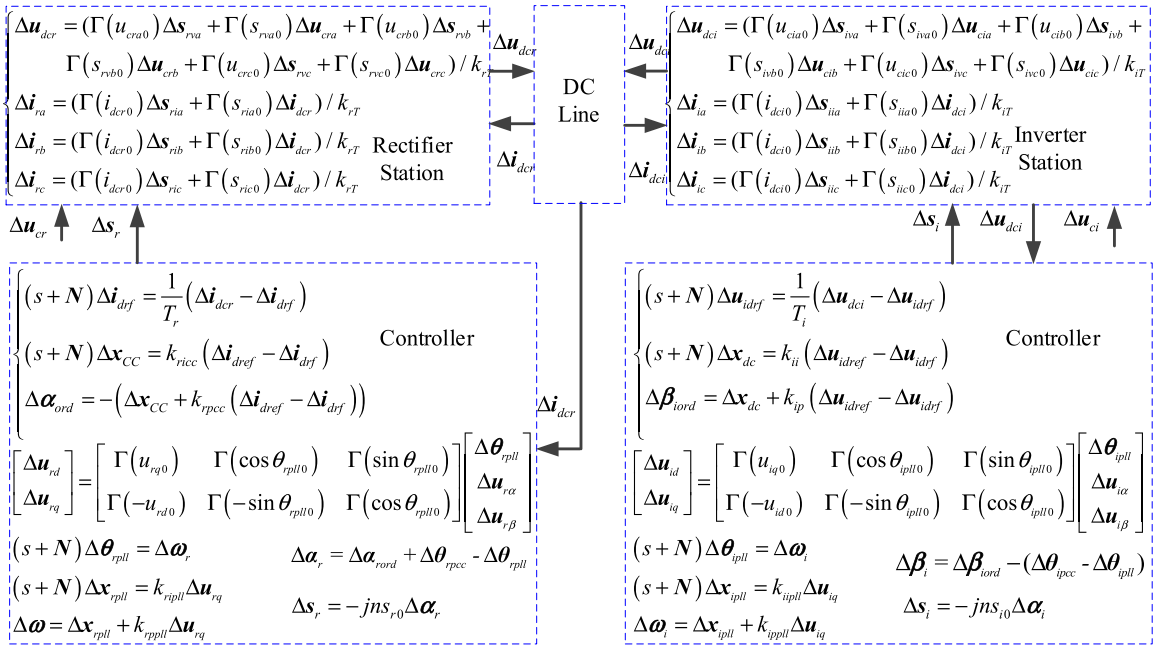

FIGURE 6. Small-signal model of modular HSS of LCC-HVDC.

TABLE 1. Constant $K_{i11} \sim K_{i89}$.

Parameter	Value
K_{i11}	$-(R_{22i}+R_{31i})/(R_{22i}R_{31i}C_{1i})$
K_{i13}	$1/(R_{22i}C_{1i})$
K_{i14}	$1/(R_{31i}C_{1i})$
K_{i15}	$-1/C_{1i}$
K_{i16}	$-1/C_{1i}$
K_{i17}	$1/C_{1i}$
K_{i18}	$-1/C_{1i}$
K_{i25}	$1/C_{2i}$
K_{i31}	$1/(R_{22i}C_{3i})$
K_{i33}	$-1/(R_{22i}C_{3i})$
K_{i35}	$1/C_{3i}$
K_{i41}	$1/(R_{31i}C_{4i})$
K_{i44}	$-1/(R_{31i}C_{4i})$
K_{i46}	$1/C_{4i}$
K_{i51}	$1/L_{2i}$
K_{i52}	$-1/L_{2i}$
K_{i53}	$-1/L_{2i}$
K_{i55}	$-R_{21i}/L_{2i}$
K_{i61}	$1/L_{3i}$
K_{i64}	$-1/L_{3i}$
K_{i71}	$-1/L_{s1i}$
K_{i77}	$(R_{s12i}+R_{s22i})/L_{s1i}$
K_{i78}	L_{s1i}
K_{i79}	L_{s1i}
K_{i87}	R_{s12i}/L_{s2i}
K_{i89}	$(R_{s12i}+R_{s22i})/L_{s2i}$

in FIGURE 7. The results of firing angle and dc current of the HSS model (blue line) are in good accordance with the results from the detailed switching model (red line).

Due to a small disturbance is applied to dc current reference i_{dref}, the dc current of rectifier station suddenly decreases in FIGURE 7 (a), resulting in a slight increase in the firing angle of the rectifier station in the initial period of disturbance in FIGURE 7 (b). The decrease of the DC current of the sending-terminal system leads to the slow decrease of the DC current of receiving-terminal system. The dynamic response in time domain is shown in FIGURE 7 (c), the firing angle of inverter station increases slowly in the initial period, and its dynamic response in time domain is shown in FIGURE 7 (d).

Initially, the system of inverter station operates at $u_{idref} = 1.0$ pu, a small disturbance is applied to u_{idref} of -0.03 pu at 0.02s, the comparison of dynamic responses between detailed switching model and modular HSS model in FIGURE 8. The results of firing angle of the HSS model (blue line) are in good accordance with the results from the detailed switching model (red line).

Through the above simulation results and analysis, it can be concluded that the modular HSS model of LCC-HVDC can reflect the dynamic characteristics of the detailed switching model to a certain extent, at the same time, it can be concluded that there exists interactions among sending-terminal and receiving-terminal system which have an influence on the stability of the system. Thus the accuracy of the small-signal model of modular HSS of LCC-HVDC is validated, in the following part, the influence of the interaction between the sending-terminal and receiving-terminal system on the stability will be analyzed by using the modular HSS model.

IV. INFLUENCE ANALYSIS OF THE INTERACTION BETWEEN THE SENDING-TERMINAL AND RECEIVING-TERMINAL SYSTEM ON THE STABILITY

The dynamic characteristics of LCC-HVDC system are determined by the interaction of converter station and AC/DC network. When the dynamic behavior of the

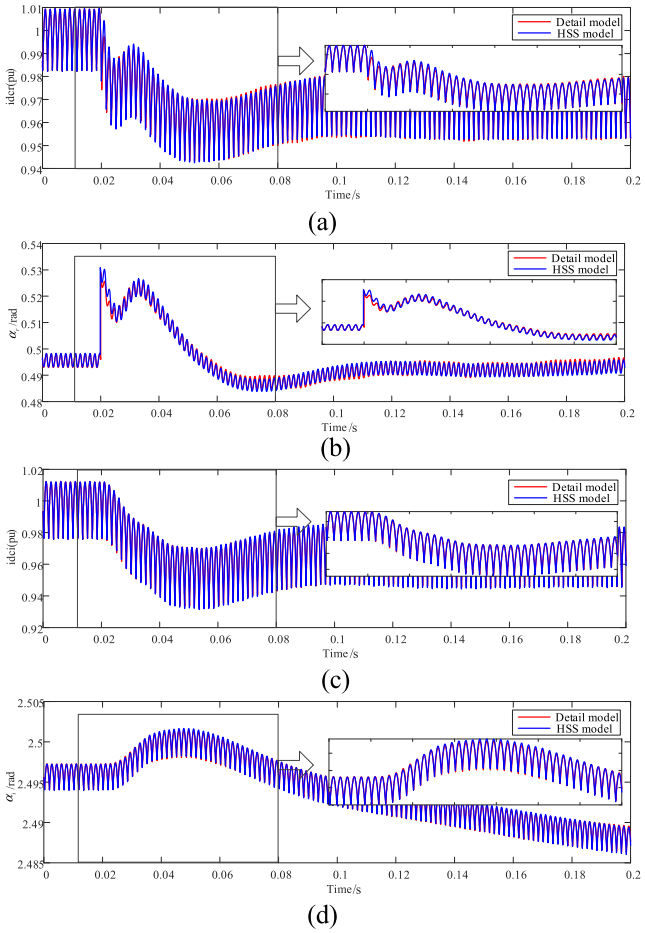

FIGURE 7. The comparison of dynamic responses between detailed switching model and modular HSS model; the response (a)-dc current and (b)-firing angle of the rectifier station, the responses (c)-dc current and (d)-firing angle of the inverter station.

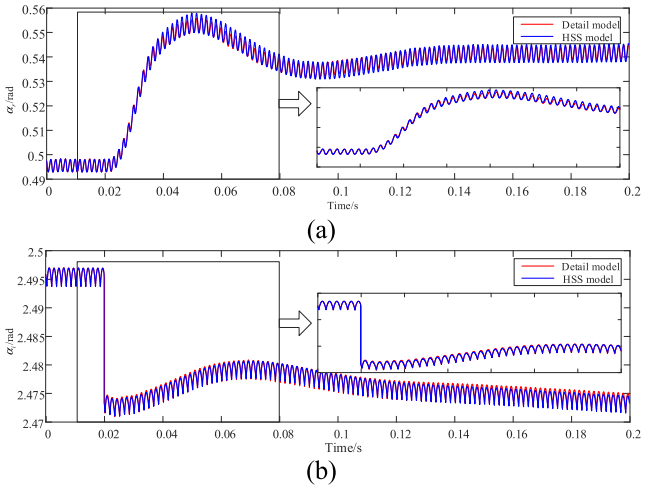

FIGURE 8. The comparison of dynamic responses between detailed switching model and modular HSS model; the response (a)-firing angle of the rectifier station, the responses (b)-firing angle of the inverter station.

sending-terminal system changes, the dynamic characteristics of receiving-terminal system also changes due to the interaction among sending-terminal and receiving-terminal system. As a current source converter, the dynamic characteristics of the AC network of the LCC-HVDC system are manifested by the AC current, when a disturbance occurred in AC network of the rectifier station, the LCC-HVDC system will have a certain dynamic with other equipment or grid, since the AC current has a mathematical relationship with the DC current similar to formula (10), the dynamic of the AC network will be transmitted to the DC line through i_{dcr}, at this time, the DC current control will to adjust the firing angle and then affect the dynamic of the AC network of the rectifier station. At the same time, according to the dynamic formula (22) of DC line, the dynamic progress of i_{dcr} will affect the dynamic progress of u_{dc}, which will lead to the DC voltage control action of the inverter station, thus the dynamic of the inverter station is affected, this is the complete interaction process in which the dynamic of inverter station is affected after the rectifier station is disturbed. Based on the modular HSS model, impact of rectifier station and inverter station's controller parameters on the interactions among sending-terminal and receiving-terminal system is analyzed.

Before analyzing, it is important to know that the modular HSS model is of infinite order, a truncation of the modular HSS model is applied, for example, if $M = 2$, the dc-component and the first and second harmonic are considered, FIGURE 9 reports an example of the modular HSS model eigenvalue locus with $M = 2$. In red are depicted the important poles and in black their translated copies. It can be noticed that for a large truncation order the eigenvalue loci result in long vertical lines of eigenvalues. In this paper, the important poles in long vertical lines of eigenvalues are selected to characterize the system.

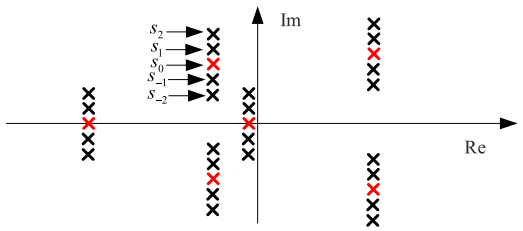

FIGURE 9. General eigenvalues locus of a HSS model. Red: significant eigenvalues. Black: translated copies.

A. IMPACT OF PLL CONTROLLER'S PARAMETERS OF SENDING-TERMINAL SYSTEM ON SYSTEM STABILITY

The PLL controller provides phase reference for firing angle control and its dynamic characteristics are one of the factors affecting the stability of the system. In the case of constant damping ratio, the influence on system stability is investigated by changing the bandwidth of the PLL controller of the system, the main state variables affecting the oscillation mode are explored by the modal participation factor, and the analytical results demonstrate that there exists interactions among sending-terminal and receiving-terminal system which have an influence on the stability of the system.

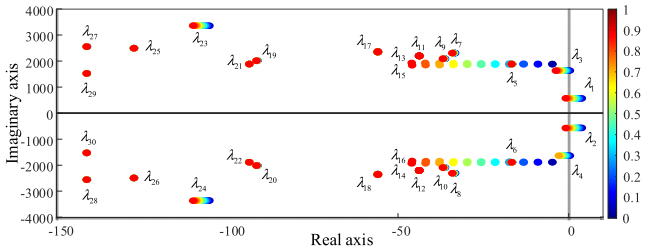

FIGURE 10. Eigenvalue locus of LCC-HVDC with varied band-width of PLL.

The influence on system stability of the modular HSS model is shown in FIGURE 10 with varied bandwidth of PLL. With the increase of the bandwidth of the PLL controller of the sending-terminal system while the damping ratio remains unchanged, the $\lambda_{5,6}$, $\lambda_{11,12}$, $\lambda_{17,18}$, $\lambda_{19,20}$, $\lambda_{21,22}$, $\lambda_{25,26}$, $\lambda_{27,28}$, $\lambda_{29,30}$ are located on the left of the imaginary axis and are largely unaffected by the bandwidth variation of PLL controller; the $\lambda_{7,8}$, $\lambda_{9,10}$, $\lambda_{13,14}$, $\lambda_{15,16}$, $\lambda_{23,24}$ monotonically move to the left half plane, showing a trend of increasing stability, among which $\lambda_{13,14}$, $\lambda_{15,16}$ are greatly influenced by the controller; the $\lambda_{1,2}$, $\lambda_{3,4}$monotonically move from the right plane to the left half plane and cross the virtual axis to the left half plane, where the largest pair of eigenvalues of the real part is (3.85±567i), and the system stability changes from unstable state to stable state. Therefore, the increase of the bandwidth of PLL will enhance the stability of the system.

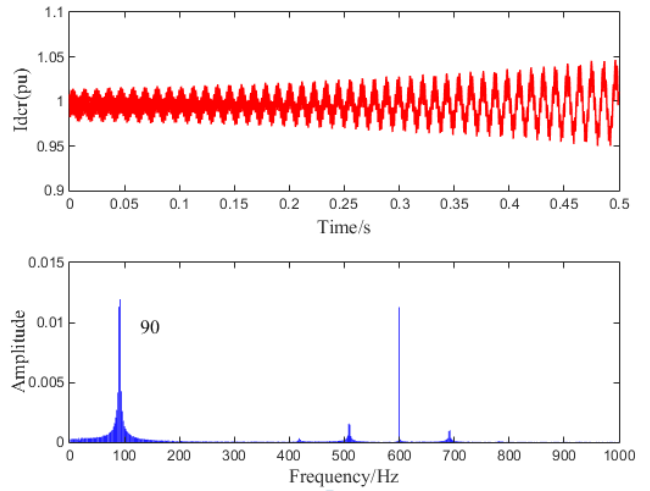

FIGURE 11. The time-domain results of DC current of rectifier station and FFT analysis.

In order to verify the correctness of the above analysis, with the case of constant damping ratio of PLL in the detailed switching model of LCC-HVDC, when the bandwidth of PLL is switched from the maximum in the above range to the minimum, the time-domain results of DC current are shown in FIGURE 11, it can be seen that the divergence appears of LCC-HVDC, and the oscillation frequency is about 90Hz. According to the analysis results of the modular HSS model of LCC-HVDC, when the bandwidth of PLL is minimum, the modular HSS model presents two pairs of eigenvalues values located in the right half plane, the eigenvalues is (3.85+567i) which the real part is the largest, and the oscillation frequency corresponding to the imaginary part is 90.24Hz, which is consistent with the oscillation frequency of the detailed switching model. These results are agreed with the modular HSS model analysis.

TABLE 2. Results of eigenvalue analysis.

Eigenvalue	f	Participation factor（>0.005）
3.85±567i	90.24	$x_{Ldcr(0)}$=0.22; $x_{L1rb(1)}$=0.102; $x_{Tr(0)}$=0.091; $x_{L1rc(1)}$=0.077; $x_{L1ra(1)}$=0.08; $x_{Cdc(0)}$=0.067; $x_{C3rb(1)}$=0.044; $x_{C3ra(1)}$=0.042; $x_{C3rc(1)}$=0.038; $x_{CC(0)}$=0.035; $x_{Ldci(0)}$=0.014;

Based on the stability analysis of eigenvalues, the modal analysis was conducted on the unstable mode of the system caused by the varied bandwidth of PLL. Table 2 shows the eigenvalues of the unstable mode caused by the parameters of PLL and the modal participation factor response results. According to Table 2, the receiving-terminal system participates in the oscillation, so it can be seen that there exists interactions among sending-terminal and receiving-terminal system which have an influence on the stability of the system.

B. IMPACT OF DC CURRENT CONTROLLER'S PARAMETERS OF SENDING-TERMINAL SYSTEM ON SYSTEM STABILITY

The DC current controller can control the DC current of the DC side of the sending-terminal system by controlling the firing angle, thus affecting the stability of the system. In the case of constant damping ratio, the influence on system stability is investigated by changing the bandwidth of the DC current controller of the system, the main state variables affecting the oscillation mode are explored by the modal participation factor, and the analytical results demonstrate that there exists interactions among sending-terminal and receiving-terminal system which have an influence on the stability of the system.

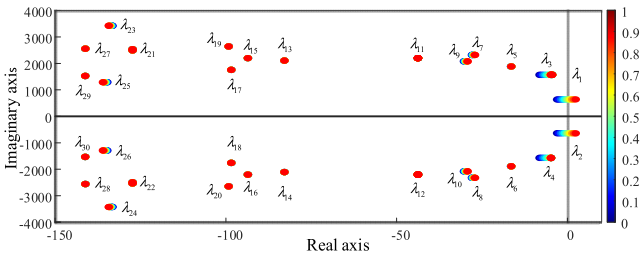

FIGURE 12. Eigenvalue trajectory of LCC-HVDC with varied bandwidth of DC current controller.

The influence on system stability of the modular HSS model is shown in FIGURE 12 with varied bandwidth of DC current controller. With the increase of the bandwidth

of the DC current controller of the sending-terminal system while the damping ratio remains unchanged, the $\lambda_{23,24}$, $\lambda_{25,26}$ monotonically move to the left half plane, showing a trend of increasing stability; the $\lambda_{5,6}$, $\lambda_{11,12}$, $\lambda_{13,14}$, $\lambda_{15,16}$, $\lambda_{17,18}$, $\lambda_{19,20}$, $\lambda_{21,22}$, $\lambda_{27,28}$, $\lambda_{29,30}$ are located on the left of the imaginary axis and are largely unaffected by the bandwidth variation of DC current controller; the $\lambda_{3,4}$, $\lambda_{7,8}$, $\lambda_{9,10}$ monotonically move to the right half plane, showing a trend of decreasing stability, but they are all located in the left half plane; the $\lambda_{1,2}$ monotonically move from the left plane to the right half plane and cross the virtual axis to the right half plane (2.45±641i), and the system stability changes from stable state to unstable state. Therefore, the increase of the bandwidth of DC current controller will weaken the stability of the system.

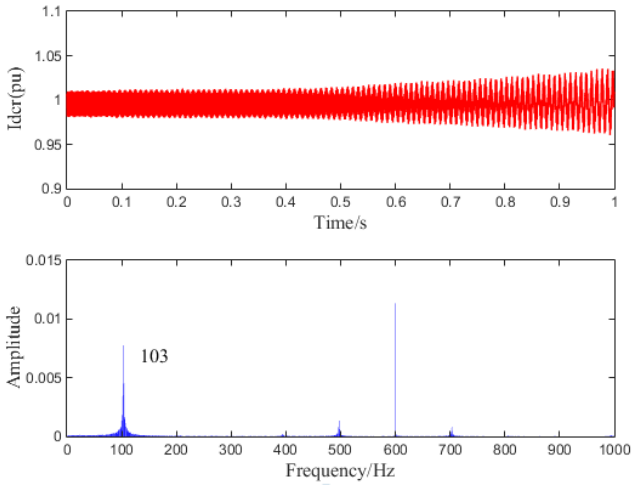

FIGURE 13. The time-domain results of DC current of rectifier station and FFT analysis.

In order to verify the correctness of the above analysis, with the case of constant damping ratio of DC current controller in the detailed switching model of LCC-HVDC, when the bandwidth of DC current controller is switched from the minimum in the above range to the maximum, the time-domain results of DC current are shown in FIGUR. 13, it can be seen that the divergence appears of LCC-HVDC, and the oscillation frequency is about 103 Hz. According to the analysis results of the modular HSS model of LCC-HVDC, when the bandwidth of DC current controller is maximum, the modular HSS model presents one pairs of eigenvalues values located in the right half plane (2.45±641i), and the oscillation frequency corresponding to the imaginary part is 102.02 Hz, which is consistent with the oscillation frequency of the detailed switching model. These results are agreed with the modular HSS model analysis.

Based on the stability analysis of eigenvalues, the modal analysis was conducted on the unstable mode of the system caused by the varied bandwidth of DC current controller. Table 3 shows the eigenvalues of the unstable mode caused by the parameters of DC current controller and the modal

TABLE 3. Results of eigenvalue analysis.

Eigenvalue	f	Participation factor（>0.005）
2.45±641i	102.02	$x_{Ldcr(0)}$=0.235; $x_{Tri(0)}$=0.129; $x_{L1rb(1)}$=0.106; $x_{L1ra(1)}$=0.09;$x_{L1rc(1)}$=0.074; $x_{CC(0)}$=0.053; $x_{Cdc(0)}$=0.05; $x_{C3rb(1)}$=0.048; $x_{C3ra(1)}$=0.046; $x_{C3rc(1)}$=0.04; $x_{Ldci(0)}$=0.006;

participation factor response results. According to Table 3, the receiving-terminal system participates in the oscillation, so it can be seen that there exists interactions among sending-terminal and receiving-terminal system which have an influence on the stability of the system.

C. IMPACT OF PLL CONTROLLER'S PARAMETERS OF RECEIVING-TERMINAL SYSTEM ON SYSTEM STABILITY

The PLL controller of receiving-terminal system provides phase reference for firing angle control and its dynamic characteristics are one of the factors affecting the stability of the system. In the case of constant damping ratio, the influence on system stability is investigated by changing the bandwidth of the PLL controller of receiving-terminal system, the main state variables affecting the oscillation mode are explored by the modal participation factor, and the analytical results demonstrate that there exists interactions among sending-terminal and receiving-terminal system which have an influence on the stability of the system.

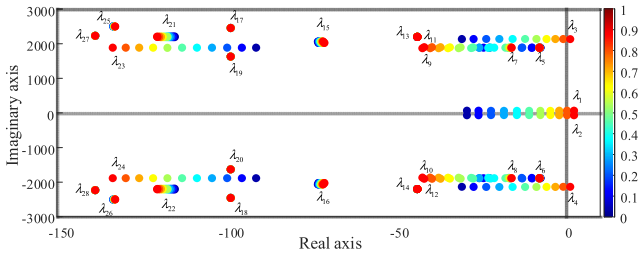

FIGURE 14. Eigenvalue locus of LCC-HVDC with varied bandwidth of PLL of receiving-terminal system.

The influence on system stability of the modular HSS model is shown in FIGURE 14 with varied bandwidth of PLL. With the increase of the bandwidth of the PLL controller of the receiving-terminal system while the damping ratio remains unchanged, the $\lambda_{5,6}$, $\lambda_{7,8}$, $\lambda_{13,14}$, $\lambda_{17,18}$, $\lambda_{19,20}$, $\lambda_{25,26}$, $\lambda_{27,28}$ are located on the left of the imaginary axis and are largely unaffected by the bandwidth variation of PLL controller; the $\lambda_{9,10}$, $\lambda_{11,12}$, $\lambda_{21,22}$, $\lambda_{23,24}$monotonically move to the left half plane, showing a trend of increasing stability, among which $\lambda_{9,10}$, $\lambda_{11,12}$, $\lambda_{23,24}$ are greatly influenced by the controller; the $\lambda_{15,16}$ monotonically move to the right half plane, showing a trend of decreasing stability, but they are all located in the left half plane; the $\lambda_{1,2}$, $\lambda_{3,4}$ monotonically

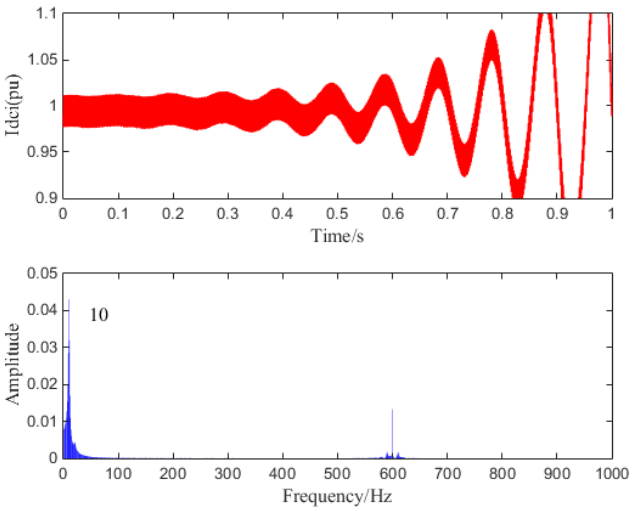

FIGURE 15. The time-domain results of DC current of inverter station and FFT analysis.

move from the left plane to the right half plane and cross the virtual axis to the right half plane, where the largest pair of eigenvalues of the real part is (1.02±64.7i), and the system stability changes from stable state to unstable state. Therefore, the increase of PLL controller's bandwidth of receiving-terminal system will weaken the stability of the system.

In order to verify the correctness of the above analysis, with the case of constant damping ratio of PLL in the detailed switching model of LCC-HVDC, when the bandwidth of PLL of receiving-terminal system is switched from the minimum in the above range to the maximum, the time-domain results of DC current of inverter station are shown in FIGURE 15, it can be seen that the divergence appears of LCC-HVDC, and the oscillation frequency is about 10Hz. According to the analysis results of the modular HSS model of LCC-HVDC, when the bandwidth of PLL is maximum, the modular HSS model presents two pairs of eigenvalues values located in the right half plane, the eigenvalues is (1.02+64.7i) which the real part is the largest, and the oscillation frequency corresponding to the imaginary part is 10.3Hz, which is consistent with the oscillation frequency of the detailed switching model. These results are agreed with the modular HSS model

TABLE 4. Results of eigenvalue analysis.

Eigenvalue	f	Participation factor（>0.005）
1.02±64.7i	10.3	$x_{PLLi2(0)}$=0.353; $x_{CC(0)}$=0.343; $x_{Ti(0)}$=0.188; $x_{Cdc(0)}$=0.165;$x_{PLLi1(0)}$=0.128; $x_{Ldci(0)}$=0.108; $x_{Vc(0)}$=0.085;$x_{Ldcr(0)}$=0.059;$x_{Tr(0)}$=0.033; $x_{Ls1ia(1)}$=0.025; $x_{Ls1ic(1)}$=0.025;$x_{Ls1ib(1)}$=0.018; $x_{Ls2ic(1)}$=0.014; $x_{Ls2ib(1)}$=0.013; $x_{Ls2ia(1)}$=0.011

analysis. When the bandwidth of PLL of receiving-terminal system is about 20.36Hz, the model has critical instability.

Based on the stability analysis of eigenvalues, the modal analysis was conducted on the unstable mode of the system caused by the varied bandwidth of PLL of receiving-terminal system. Table 4 shows the eigenvalues of the unstable mode caused by the parameters of PLL and the modal participation factor response results. According to Table 4, the sending-terminal system participates in the oscillation, so it can be seen that there exists interactions among sending-terminal and receiving-terminal system which have an influence on the stability of the system.

V. CONCLUSION

Based on harmonic state space theory, this paper focuses on the dynamic stability of LCC-HVDC system, and studies the influence of controller's parameters of the modular HSS model of LCC-HVDC and its interaction on the system stability. The innovation and contribution of this paper can be summarized as follows:

1) The HSS modeling of LCC-HVDC system is carried out, and the idea of modular HSS modeling of LCC-HVDC is proposed, which is conducive to the establishment and expansion of the model. The small-signal model of modular HSS of LCC-HVDC is established, which includes both sending-terminal and receiving-terminal system.

2) Based on the small-signal model of modular HSS of LCC-HVDC with sending-terminal and receiving-terminal system, the stability analysis is carried out to explore the influence of controller's parameters on system stability. By means of modal analysis, it is found that the oscillation modes are mainly dominated by the state variables of controller of sending-terminal system, filter, DC network and AC network of sending-terminal and receiving-terminal system. The results show that there exists interactions among sending-terminal and receiving-terminal system which have an influence on the stability of the system.

REFERENCES

[1] M. Callavik, M. Larsson, and S. Stoeter, "Powering the world, ABB review, special report 60 years of HVDC," Tech. Rep., Jul. 2014, pp. 6–9.
[2] Y. Qi, H. Zhao, S. Fan, A. M. Gole, H. Ding, and I. T. Fernando, "Small signal frequency-domain model of a LCC–HVDC converter based on an infinite series-converter approach," *IEEE Trans. Power Del.*, vol. 34, no. 1, pp. 95–106, Feb. 2019.
[3] H. Xiao, Y. Li, and T. Lan, "Sending end AC faults can cause commutation failure in LCC–HVDC inverters," *IEEE Trans. Power Del.*, vol. 35, no. 5, pp. 2554–2557, Oct. 2020.
[4] X. Yuan, S. Cheng, and J. Hu, "Multi-time scale voltage and power angle dynamics in power electronics dominated large power systems," *Proc. Chin. Soc. Elect. Eng.*, vol. 36, no. 19, pp. 5145–5154, Oct. 2016.
[5] L. Mingjie, "Characteristic analysis and operational control of large-scale hybrid UHV AC/DC power grids," *Power Syst. Technol.*, vol. 40, no. 4, pp. 985–991, 2016.
[6] J. Lu, X. Yuan, J. Hu, M. Zhang, and H. Yuan, "Motion equation modeling of LCC–HVDC stations for analyzing DC and AC network interactions," *IEEE Trans. Power Del.*, vol. 35, no. 3, pp. 1563–1574, Jun. 2020.
[7] Y. Shu, G. Chen, Z. Yu, J. Zhang, C. Wang, and C. Zheng, "Characteristic analysis of UHVAC/DC hybrid power grids and construction of power system protection," *CSEE J. Power Energy Syst.*, vol. 3, no. 4, pp. 325–333, Dec. 2017.

[8] J. Tu, J. Zhang, G. Bu, J. Yi, Y. Yin, and J. Jia, "Analysis of the sending-side system instability caused by multiple HVDC commutation failure," *CSEE J. Power Energy Syst.*, vol. 1, no. 4, pp. 37–44, Dec. 2015.
[9] A. Zheng, C. Guo, P. Cui, W. Jiang, and C. Zhao, "Comparative study on small-signal stability of LCC–HVDC system with different control strategies at the inverter station," *IEEE Access*, vol. 7, pp. 34946–34953, 2019.
[10] Y. Dong, J. Ma, S. Wang, T. Liu, X. Chen, and H. Huang, "An accurate small signal dynamic model for LCC–HVDC," *IEEE Trans. Appl. Supercond.*, vol. 31, no. 8, pp. 1–6, Nov. 2021.
[11] A. R. Beig and M. S. J. Asghar, "Performance evaluation and reliability of flexible asynchronous AC link and LCC–HVDC link under fault conditions," *IEEE Access*, vol. 8, pp. 120562–120574, 2020.
[12] Y. C. Choo, A. P. Agalgaonkar, K. M. Muttaqi, S. Perera, and M. Negnevitsky, "Subsynchronous torsional interaction behaviour of wind turbine-generator unit connected to an HVDC system," in *Proc. 36th Annu. Conf. IEEE Ind. Electron. Soc.*, Nov. 2010, pp. 996–1002.
[13] M. Zhang and X. Yuan, "Modeling of LCC HVDC system based on mass-damping-spring concept," in *Proc. IEEE Power Energy Soc. Gen. Meeting (PESGM)*, Jul. 2016, pp. 1–5.
[14] M. Daryabak, S. Filizadeh, J. Jatskevich, A. Davoudi, M. Saeedifard, V. K. Sood, J. A. Martinez, D. Aliprantis, J. Cano, and A. Mehrizi-Sani, "Modeling of LCC–HVDC systems using dynamic phasors," *IEEE Trans. Power Del.*, vol. 29, no. 4, pp. 1989–1998, Aug. 2014.
[15] C. Liu, A. Bose, and P. Tian, "Modeling and analysis of HVDC converter by three-phase dynamic phasor," in *Proc. IEEE PES Gen. Meeting | Conf. Expo.*, Jul. 2014, pp. 1–10.
[16] M. Daryabak, S. Filizadeh, and A. B. Vandaei, "Dynamic phasor modeling of LCC–HVDC systems: Unbalanced operation and commutation failure," *Can. J. Electr. Comput. Eng.*, vol. 42, no. 2, pp. 121–131, Jun. 2019.
[17] H. Liu and J. Sun, "Modeling and analysis of DC-link harmonic instability in LCC HVDC systems," in *Proc. IEEE 14th Workshop Control Modeling Power Electron. (COMPEL)*, Jun. 2013, pp. 1–9.
[18] K. Jiang, C. Kan, D. Liu, P. Xiong, Y. Kang, and C. Ye, "Modeling of LCC–HVDC considering sending/receiving-terminal system using harmonic state space method," in *Proc. IEEE Sustain. Power Energy Conf. (iSPEC)*, Dec. 2021, pp. 2732–2737.
[19] E. Mollerstedt and B. Bernhardsson, "Out of control because of harmonics-an analysis of the harmonic response of an inverter locomotive," *IEEE Control Syst. Mag.*, vol. 20, no. 4, pp. 70–81, Aug. 2000.
[20] J. Kwon, X. Wang, F. Blaabjerg, C. L. Bak, A. R. Wood, and N. R. Watson, "Harmonic instability analysis of a single-phase grid-connected converter using a harmonic state-space modeling method," *IEEE Trans. Ind. Appl.*, vol. 52, no. 5, pp. 4188–4200, Sep./Oct. 2016.
[21] Z. Xu, B. Li, S. Wang, S. Zhang, and D. Xu, "Generalized single-phase harmonic state space modeling of the modular multilevel converter with zero-sequence voltage compensation," *IEEE Trans. Ind. Electron.*, vol. 66, no. 8, pp. 6416–6426, Aug. 2019.
[22] J. Lyu, X. Zhang, X. Cai, and M. Molinas, "Harmonic state-space based small-signal impedance modeling of a modular multilevel converter with consideration of internal harmonic dynamics," *IEEE Trans. Power Electron.*, vol. 34, no. 3, pp. 2134–2148, Mar. 2019.
[23] M. Szechtman, T. Wess, and C. V. Thio, "A benchmark model for HVDC system studies," in *Proc. Int. Conf. AC DC Power Transmiss.*, Sep. 1991, pp. 374–378.

KEZHENG JIANG received the M.S. degree from the Huazhong University of Science and Technology, China, in 2021. His current research interests include the modeling and analysis of HVDC and instability issues in power systems.

PAN HU (Senior Member, IEEE) received the Ph.D. degree from Wuhan University, China, in 2018.

His current research interest includes the economic and stability analysis of power systems.

KAN CAO received the Ph.D. degree from Chongqing University, China, in 2012. His current research interests include HVDC applications, modeling, analysis, and control of power electronized power systems.

DAN LIU received the M.S. degree from the Huazhong University of Science and Technology, China, in 2013. His current research interest includes the stability analysis of renewable energy generations.

CHANG YE received the Ph.D. degree from the Huazhong University of Science and Technology, China, in 2019. His current research interests include the stability analysis of power electronic devices, such as wind turbines, PV, and HVDC.